

A NOVEL ACCURATE PATTERN FITTING OF NOISY IRREGULAR BEAM DATA FOR THE PLANCK SPACE TELESCOPE

Oscar Borries, Frank Jensen, Per Heighwood Nielsen
TICRA
Laederstraede 34, 1201 Copenhagen, Denmark

Jan Tauber, Arturo Martín-Polegre
ESTEC
Keplerlaan 1, 2200 AG Noordwijk, The Netherlands

ABSTRACT

Kriging fitting, originally developed for geological exploitation, is here applied for fitting an expected pattern to noisy, irregular in-flight measurements of a satellite antenna.

The noise level in in-flight measurements is often so high that only the central part of the main beam appears. By the Kriging method, first a characteristic function, the regression model, is fitted to the measurements. For the main beam this is chosen to be described by a general second order polynomial. To this is added a more detailed correlation model which represents realistic deviations from the regression model but filters out the fast variations of the noise.

The method is applied on simulated measurements on the Planck RF telescope and the presented results show a considerable reduction of the noise floor of the pattern; even beam details invisible in the original measurements (a shoulder) are revealed by the pattern fitting¹.

Keywords: In-Flight Testing, Pattern Reconstruction, Kriging, mm-Wave, Satellite

1. Introduction

Testing of a satellite borne antenna after launch is desirable in many cases. For the Planck Space Telescope the operating temperature of the reflector antenna is 40K and satisfactory testing on the ground could not be achieved as extremely accurate knowledge of the antenna pattern is crucial for the scientific results.

The Planck satellite [1] is a spinning satellite with a double reflector which scans the celestial sphere for weak signals from the Big Bang and focuses these on the focal

plane with 47 detectors operating from 30 to 857 GHz, cf. Figure 1.

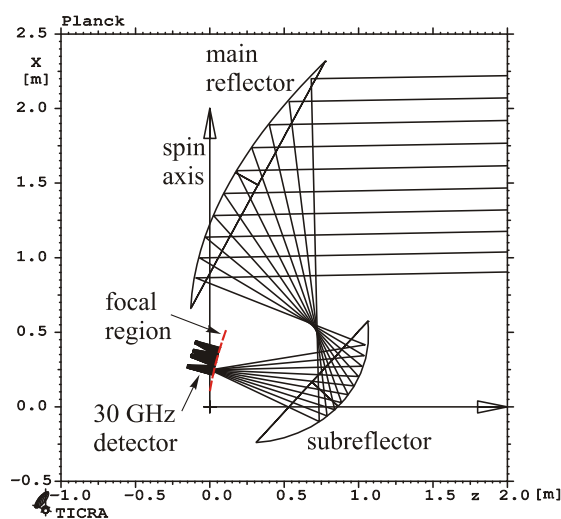


Figure 1 – The Planck double reflector antenna system with two ellipsoidal mirrors (aplanatic configuration).

From the antenna pattern obtained by the in-flight testing it is possible to deduce information about the antenna such as possible defects of the reflector surface which may then be used to predict a better pattern. A method based on this technique and further combining data from detectors at different frequency bands has previously been presented [2]. Further details regarding the spinning antenna may also be found here.

In the present paper we will describe a new powerful technique – based on a Kriging algorithm – for reconstructing the pattern measured by in-flight testing of the Planck antenna system. In the in-flight testing Mars and Jupiter are scanned as reference sources but noise generated by the sampled planet and by the temperature of the detector (though down to 0.1K) hampers the measure-

¹ The work presented in this paper has been carried out under ESTEC Contract No. 18395/NL/NB

ments. In the new reconstruction technique described here the influence of the noise is reduced considerably.

The measurements and the method are shortly presented in Sections 2 and 3 and a more detailed description of the algorithm is presented in Section 4. The results are presented in Section 5 and the conclusions are found in Section 6.

2. The measurements

For the Planck Telescope, the in-flight measurements are characterized by a large number of measurements in an irregular pattern as a consequence of the scanning performed by the rotating satellite. Furthermore, the signals are measured several times in nearly the same directions. On the other hand, the measurements contain intrinsic noise, particularly at the lowest frequencies. The 30 GHz LFI detector will be used as example in this presentation. Results will further be given for a 353 GHz HFI detector.

As the disclosure of in-flight measured data is contractually not allowed, all presented results are based on simulations of realistic data.

An example of the directions of measurements of Jupiter covering the main beam area for the 30 GHz LFI detector is shown in Figure 2. The in total 41677 directions are found distributed in ‘lines’ along the scan direction. The measured pattern is presented in Figure 4.

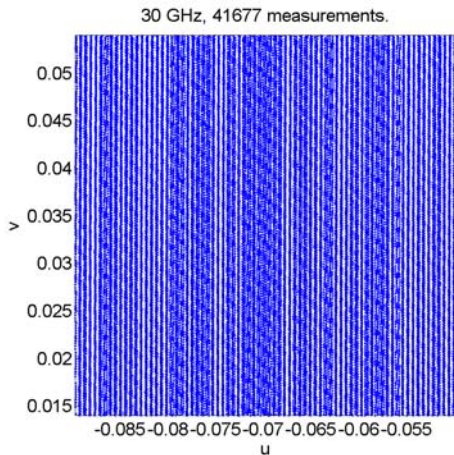


Figure 2 - Directions of measurements, each given as a dot, within the main beam of a 30 GHz detector. Note the distribution in lines along the scan direction v .

3. Method

The goal is to find a model from the measurements for the true antenna pattern. As the measurements are noisy, the model shall not follow the measurements strictly, but pre-

sent a pattern description in which the noise is smoothed out while minor, but realistic, field variations are reconstructed.

To reduce the noise, and achieve a model in a regular grid, a two-stage fitting algorithm has been developed, exploiting the spatial dependency of the measurements. The first stage consists of a rather crude filter, the purpose of which is to reduce the noise as well as the amount of data. The second stage is the Kriging fitting model. This stage is inspired by the implementation in the Matlab Kriging toolbox DACE [3,4], modified to employ fitting and implemented in FORTRAN with focus on memory efficiency and stability.

4. Algorithm

Mathematically, we are given m measurements of field values z in directions (u,v) , where

$$\begin{aligned} u &= \sin\theta \cos\varphi \\ v &= \sin\theta \sin\varphi \end{aligned}$$

with θ and φ being usual spherical coordinates and $\theta = 0$, corresponding to $(u,v) = (0,0)$, is close to the direction of the beam.

The samples are noisy and irregularly distributed, but have a spatial dependency, such that the closer two measurements are in the uv -plane, the greater the correlation between their field values.

With the datasets we are considering, the number of measurements m is far too large to employ the Kriging algorithm directly as the chief computational costs of computing the Kriging model is the Cholesky factorization of a $m \times m$ matrix for which the number of operations scales as $\mathcal{O}(m^3)$. For the 30 GHz dataset, $m = 41677$, and thus a data reduction is needed. Furthermore, experiments have shown that Kriging fitting performs poorly on datasets affected by serious noise, particularly for low-dimensional data. Therefore, a crude spatial filter is initially employed.

4.1 Filter

The purpose of the filter is to reduce the noise as well as the amount of data. This may be done by an averaging as it may be assumed that the noise is symmetrically distributed with an average of zero.

The directions (u,v) of the measurements is divided into a grid and the output of the filter is the average of the measurements within each cell of this grid. When the cells are large each cell will keep a large amount of data and the averaging will give a good noise reduction. On

the other hand, field variations within a cell cannot be represented and the cells shall not be too large.

The Nyquist criterion states that all field variations will be measured when the sampling is carried out with a spacing which does not exceed λ/D , λ being the wavelength and D the diameter of the radiating aperture. This is the theoretical maximum sample spacing. For a good interpolation of the field the sample spacing shall be at least four times smaller, i.e. $0.25\lambda/D$. However, the request for fine pattern details suggests an even denser spacing of the data points such as $0.1\lambda/D$. In the present case the 41677 samples cover a total region which in u and v is about $5\lambda/D$. Averaging the data within cells being $0.1\lambda/D$ in both u and v then results in 2500 cells with, in average, 17 data points in each cell. This choice is found to be a good compromise between noise reduction and the ability to detect pattern details. An example of the filtering is illustrated in Figure 3.

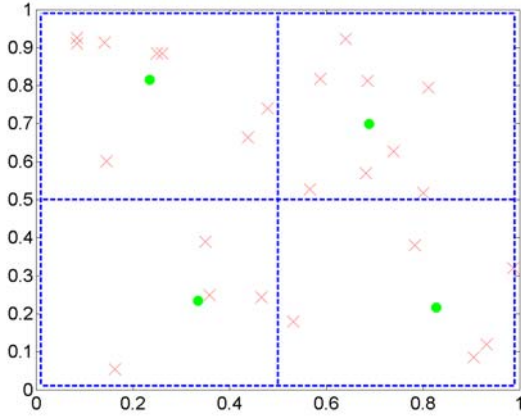


Figure 3 - A mini-example of the filter. The blue lines represent four cells of the grid, separated by $0.1\lambda/D$. The red crosses are the measurements, and the green dots are the result of the filter - representing the average of the samples inside each cell.

4.2 Kriging

The method of Kriging exploits a supposed spatial dependency in a set of samples to impose additional requirements on the fit. In its simplest form, it basically involves the fitting of a correlation model to a sample set - it was in this form Danie Krige [5] introduced it. Later work by several people, most notably G. Matheron [6], formalized it further and introduced several variations of the model, including the Universal Kriging model applied here. Its use in modelling deterministic behaviour was introduced by the landmark paper [7], allowing widespread use of the method which was previously restricted to the geostatistical community. Theoretically, the key

strength of the Kriging predictor is that amongst all linear and unbiased estimators, it minimizes the expected error [8, p. 60]. In practice, it has several other advantages which have prompted its use in the present scenario - most notably, it yields a smooth model and requires no special considerations when faced with irregularly distributed data. Also, its use of a global regression model and a local correlation model allows for surprisingly good accuracy when applied correctly.

4.2.1 Model

Given is a set of m measured field values z_i in directions (u_i, v_i) , $i = 1, \dots, m$. The process is started by normalizing the data by subtracting the average value and dividing by the standard deviation for each of the variables u , v and z . In this way they each have an average of zero and a standard deviation of one whereby better numerical and statistical properties are obtained [3,8].

Mathematically, we arrange the normalized field values in a vector $\mathbf{z} = (z_1, z_2, \dots, z_m)^T$ and the normalized measurement directions similarly in $\mathbf{X} = (\mathbf{x}_1, \mathbf{x}_2, \dots, \mathbf{x}_m)^T$ where the i 'th row \mathbf{x}_i describes the direction (u_i, v_i) .

Inspired by [7], a model is adopted that expresses the field $z(u, v)$ by a sum of a regression model F and a correlation model S such that the field model is given by

$$z(u, v) = F(u, v) + S(\rho_u, \rho_v, u, v) \quad (4.1)$$

Here, the *regression* model, $F(u, v)$, shall be restricted to a polynomial² in u and v . The number n of coefficients, β_j , $j=1, 2, \dots, n$, needed for describing the polynomial depends on the order of the polynomial. In our case we found that the use of second order polynomials provided the best results, yielding $n = 6$:

$$F(u, v) = \beta_1 + \beta_2 u + \beta_3 v + \beta_4 u^2 + \beta_5 v^2 + \beta_6 uv \quad (4.2)$$

The polynomial term with coefficient β_j is denoted $f_j(u, v)$ (i.e. $f_1(u, v) = 1, \dots, f_6(u, v) = uv$) and Eq. (4.2) may in general be expressed as

$$F(u, v) = \sum_1^n \beta_j f_j(u, v) \quad (4.3)$$

The *correlation* model, $S(\rho_u, \rho_v, u, v)$, is a Gaussian model controlling the correlation between measurements according to the distance between the measurement directions. Here, ρ_u and ρ_v act as scaling parameters in the uv -plane as explained below.

This allows us to express Eq. (4.1) as a matrix expression

² In general, other linear expressions may be applied for the regression model.

$$\mathbf{z} = \mathbf{F}\boldsymbol{\beta} + \boldsymbol{\Phi}(\boldsymbol{\rho})\boldsymbol{\alpha} \quad (4.4)$$

Where \mathbf{F} is the *regression* matrix, i.e. the element F_{ij} represents the j 'th polynomial f_j evaluated at the i 'th measurement direction $\mathbf{x}_i = (u_i, v_i)$

$$F_{ij} = f_j(\mathbf{x}_i), \quad i = 1, 2, \dots, m, \quad j = 1, 2, \dots, n$$

and $\boldsymbol{\beta}$ is a vector with the polynomial coefficients

$$\boldsymbol{\beta} = (\beta_1, \beta_2, \dots, \beta_n)^T.$$

The elements Φ_{ij} of the *correlation* matrix $\boldsymbol{\Phi}$ are given as the correlation between the i 'th and the j 'th measurement direction according to the scaling parameters $\boldsymbol{\rho}$

$$\Phi_{ij} = r(\boldsymbol{\rho}, \mathbf{x}_i, \mathbf{x}_j), \quad i, j = 1, 2, \dots, m.$$

The correlation is expressed as a Gaussian correlation

$$r(\boldsymbol{\rho}, \mathbf{x}_i, \mathbf{x}_j) = \exp\left[-\rho_u (u_i - u_j)^2\right] \exp\left[-\rho_v (v_i - v_j)^2\right] \quad (4.5)$$

The first term in Eq. (4.4) expresses a model of the measured field as a rather crude approximation by a polynomial with n coefficients $\boldsymbol{\beta}$. To this is added the correlation functions r in the form of Gaussian hats of widths ρ_u and ρ_v in u and v , respectively, and amplitudes adjusted by the weights $\boldsymbol{\alpha} = (\alpha_1, \alpha_2, \dots, \alpha_m)^T$ such that the model agrees with the measured field values at the measurement points.

This is a strict model which may be applied for interpolation, but it does not take into account that the measurements may be defective in any way. To achieve a realistic fitting model, we therefore add a constant γ , ($\gamma > 0$) to the diagonal elements of $\boldsymbol{\Phi}$, yielding the final model

$$\mathbf{z} = \mathbf{F}\boldsymbol{\beta} + [\boldsymbol{\Phi}(\boldsymbol{\rho}) + \gamma\mathbf{I}]\boldsymbol{\alpha} \quad (4.6)$$

\mathbf{I} being the identity matrix of order m . The i 'th diagonal element of $\boldsymbol{\Phi}$ is the autocorrelation for the i 'th measurement, $\Phi_{ii} = 1$ cf. Eq. (4.5). By adding γ to the diagonal elements of the matrix, we give the model freedom to follow a more likely path following, but not passing through, the measurement points.

Computation of the parameters $\boldsymbol{\beta}$, $\boldsymbol{\rho}$, $\boldsymbol{\alpha}$ and γ is by far the most tricky aspect of the implementation, as great care needs to be taken to ensure numerically stable and computationally efficient results. Principally $\boldsymbol{\beta}$, the coefficients to the polynomial $F(u, v)$ in Eq. (4.3), is first determined by solving

$$\min \|\mathbf{z} - \mathbf{F}\boldsymbol{\beta}\|_2 \quad (4.7)$$

This is an over-determined system fitting the polynomial $F(u, v)$ to the measured data. The terms of Eq. (4.6) are then rearranged

$$\mathbf{z} - \mathbf{F}\boldsymbol{\beta} = [\boldsymbol{\Phi}(\boldsymbol{\rho}) + \gamma\mathbf{I}]\boldsymbol{\alpha} \quad (4.8)$$

and $\boldsymbol{\alpha}$ is determined by a matrix inversion; $\boldsymbol{\rho}$ and γ may be determined automatically by a Maximum Likelihood Estimate, details may be found in [3,4,9]. The key point in the method is the application of a model, Eq. (4.6), which consists of a global regression part and a local correlation part.

4.2.2 Predictor

Having determined the model, we can predict the field value z at an arbitrary direction $\mathbf{x} = (u, v)$ as [3, (2.16)]

$$z(u, v) = F(u, v) + \mathbf{r}(\boldsymbol{\rho}, \mathbf{x}, \mathbf{X}) \cdot \boldsymbol{\alpha} \quad (4.9)$$

where $F(u, v)$, the regression part, is given by Eq. (4.3). The last term, the correlation part, is the dot product of the vector \mathbf{r} – for which the j 'th element $r_j(\boldsymbol{\rho}, \mathbf{x}, \mathbf{x}_j)$ is the value of the correlation, Eq. (4.5), between the actual direction \mathbf{x} and the j 'th measurement direction \mathbf{x}_j – and the vector $\boldsymbol{\alpha}$ with the weights of the correlation functions.

This yields a prediction in the normalized space which has to be scaled back to the original space according to the normalization mentioned at the beginning of Section 4.2.1. This is simply carried out by multiplying by the standard deviation and next adding the average value of the measured field values.

5 Results

The beam of the 30 GHz LFI detector is simulated measuring Jupiter. The main-beam pattern is calculated by GRASP [10] applying Physical Optics. To this is added a realistic noise at 14 dB (rms) below peak. The resulting simulated pattern is shown in the 3D view in Figure 4.

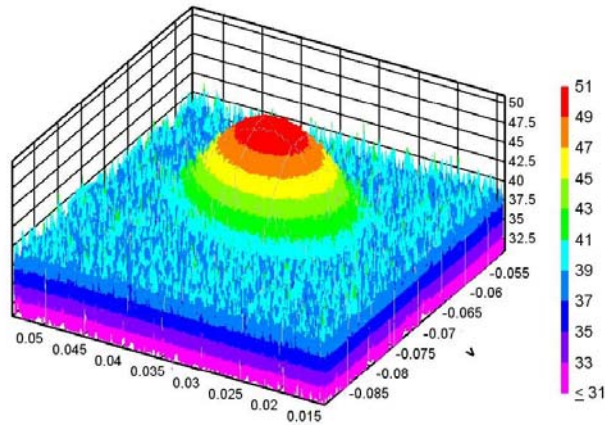


Figure 4 - Simulated main beam with noise for the 30 GHz detector LFI-27-S.

Applying the algorithm with a cell size for the filtering of $0.1\lambda/D$ and Kriging parameters as computed by the algorithm, yields the result shown in Figure 5 clearly demonstrating the reduction of the noise.

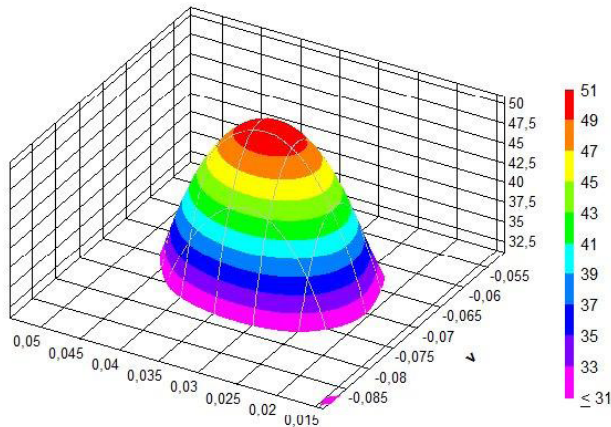


Figure 5 - Noise filtered and Kriging fitted main beam for the 30 GHz detector LFI-27-S.

The fitted simulated main beam is compared to the noiseless simulated beam in Figure 6. The main shapes of the contour curves down to the noise level at 14 dB are very well regenerated; further, the noise floor is reduced to about 20 dB below peak and the noise is not dominant until levels as low as 25 dB below peak that.

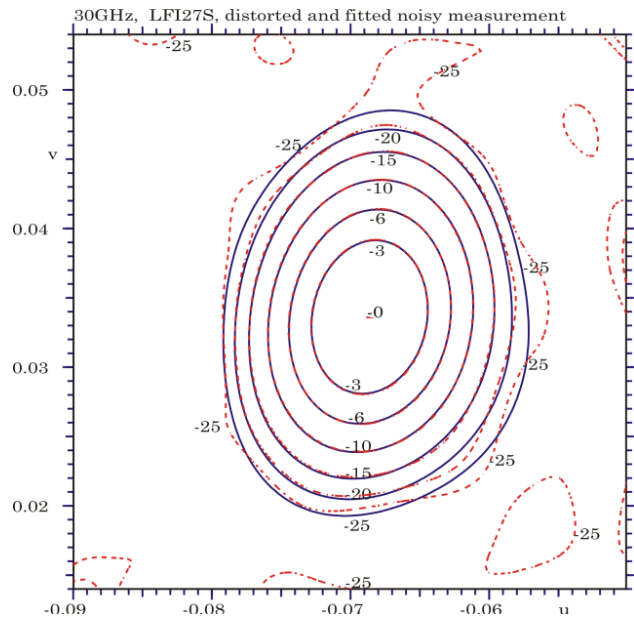


Figure 6 - Noise filtered and Kriging fitted main beam, shown in dashed red curves, compared with noiseless pattern for the 30 GHz detector, LFI-27-S, shown in solid blue curves.

The runtime for the pattern fitting is in seconds giving possibility for some interactive steps in the modelling for solving Eq.(4.6).

The improvements obtained for a High Frequency Instruments are exemplified by a 353 GHz detector. The beam width is then about 12 times less than in the previous example due to the 12 times higher frequency. This implies that the region of measurements in the uv -space is reduced by a factor 144 and so is the number of available field measurements. The number of cells is kept constant resulting in 1.4 points per cell in average. The reduction in the noise by the filter is therefore less pronounced. On the other hand, the noise in the measurements is lower, namely at 26 dB below peak.

The simulated measurements of Jupiter show a simple main beam, Figure 7, but after the filtering and the pattern fitting with the Kriging technique the pattern of Figure 8 is obtained, and now a shoulder appears at low u - and v -values. The shoulder is real which can be seen in the comparison to the reference pattern, Figure 9. In this case the noise level has been reduced to about -28 dB.

The Kriging fitted beams are used directly in the retrieval of the geometrical information on the Planck reflectors. Due to the very precise fitting and noise reduction a larger dynamic range of the measured beams can be utilized in the retrieval giving much more information about the telescope mirror alignment and surface deformations. Furthermore, it is much simpler to calculate the main

beam characteristics, such as beam peak, half power ellipticity and efficiency in the regular grid generated by the Kriging.

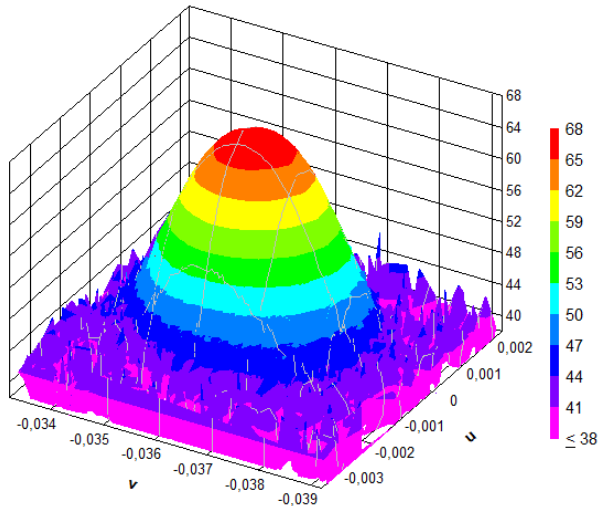


Figure 7 - Simulated main beam with noise for the 353 GHz detector HFI-353-1.

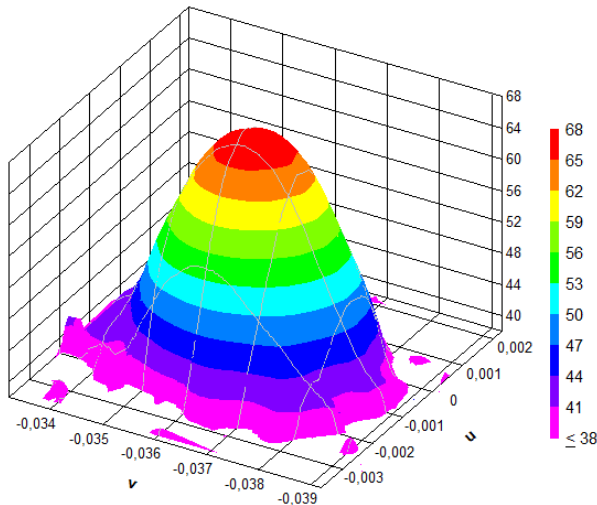


Figure 8 - Noise filtered and Kriging fitted main beam for the 353 GHz detector HFI-353-1.

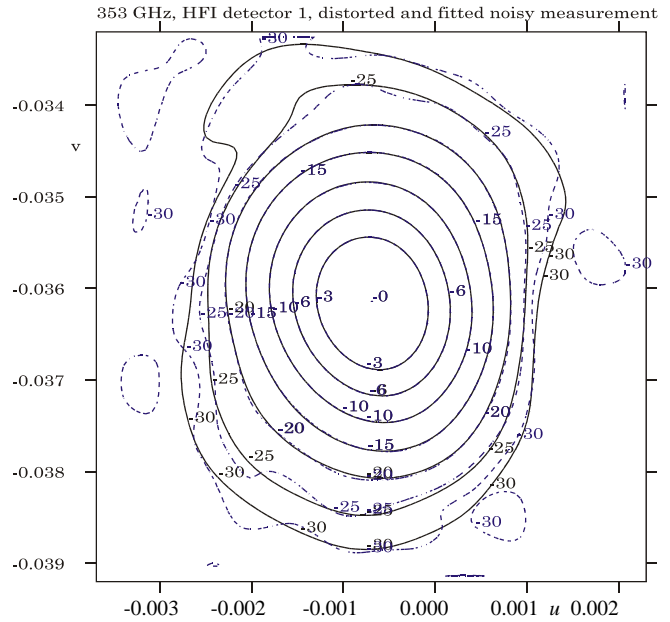


Figure 9 - Noise filtered and Kriging fitted main beam for the 353 GHz detector HFI-353-1 shown as dashed curves and compared to the noiseless pattern shown as solid curves.

6. Conclusions

The algorithm presented for reconstructing an antenna main-beam pattern from noisy measurements demonstrates considerably improved pattern information with a reduced noise level. The method starts with a crude filtering of the data utilizing the availability of a large amount of data. The key point of the method is, however, the following step with a Kriging fitting applying a global regression part overlaid with a local correlation part.

The Kriging fitting hereby exploits the spatial dependency of the data, namely that it represents a main beam which is primarily fitted by a second order polynomial. In addition, the model allows deviations from this primary model by including a correlation term representing the correlation between the measured points.

Furthermore, although not discussed here, the runtimes are very reasonable, in the order of seconds, allowing a more interactive approach to the modelling process. In conclusion, the algorithm presented improves upon previous algorithms and will be vital in the in-flight geometry retrieval of the Planck space telescope.

References

- [1] C. Bertout, C. and T. Forville (Eds.), Special Issue: Pre-launch status of Planck mission, *Astronomy & Astrophysics*, Vol. 520, 15 Sep 2010.

- [2] F. Jensen, P. H. Nielsen, J. Tauber, and A. Martín-Polegre, "Improved in-flight pattern retrieval by reflector deformation fitting", Proc. Antenna Measurement Techniques Association 32nd Annual Symposium, Atlanta, Georgia, USA, 10-15 October 2010.
- [3] S. N. Lophaven, H. B. Nielsen, and J. Søndergaard, "DACE, a MATLAB Kriging toolbox", Version 2.0, IMM, DTU, Tech. Rep. IMM-TR-2002-12, 2002, available online at <http://www2.imm.dtu.dk/~hbn/dace/dace.pdf>.
- [4] S. N. Lophaven, H. B. Nielsen, and J. Søndergaard, "Aspects of the MATLAB toolbox DACE", IMM, DTU, Tech. Rep. IMM-REP-2002-13, 2002, available online at <http://www.imm.dtu.dk/~hbn/publ/TR0213.ps>.
- [5] D. G. Krige, "A statistical approach to some basic mine valuation problems on the Witwatersrand," Journal of the Chemical, Metallurgical and Mining Engineering Society of South Africa, pp. 119–139, 1951.
- [6] G. Matheron, "Principles of Geostatistics," Economic Geology, pp. 1246–1266, 1963.
- [7] J. Sacks, W. Welch, T. Mitchell, and H. Wynn, "Design and analysis of computer experiments," Stat. Sci., vol. 4, pp. 409–435, 1989.
- [8] T. J. Santner, B. J. Williams, and W. I. Notz, The Design and Analysis of Computer Experiments, 1st ed., ser. Springer Series in Statistics. Springer, 2003.
- [9] A. Forrester, A. Sobester, and A. Keane, Engineering Design via Surrogate Modelling, 1st ed. Wiley, 2007.
- [10] K. Pontoppidan, GRASP9 Technical Description, 1st ed. TICRA, 2005.